Accurate predictive model of band gap with selected important features based on explainable machine learning

Joohwi Lee^{1,*} and Kaito Miyamoto¹

¹Toyota Central R&D Labs., Inc., Yokomichi 41-1, Nagakute, Aichi, 480-1192, Japan

ABSTRACT

In the rapidly advancing field of materials informatics, nonlinear machine learning models have demonstrated exceptional predictive capabilities for material properties. However, their black-box nature limits interpretability, and they may incorporate features that do not contribute to—or even deteriorate—model performance. This study employs explainable ML (XML) techniques, including permutation feature importance and the SHapley Additive exPlanation, applied to a pristine support vector regression model designed to predict band gaps at the GW level using 18 input features. Guided by XML-derived individual feature importance, a simple framework is proposed to construct reduced-feature predictive models. Model evaluations indicate that an XML-guided compact model, consisting of the top five features, achieves comparable accuracy to the pristine model on in-domain datasets (0.254 vs. 0.247 eV) while demonstrating superior generalization with lower prediction errors on out-of-domain data (0.461 vs. 0.341 eV). Additionally, the study underscores the necessity for eliminating strongly correlated features (correlation coefficient greater than 0.8) to prevent misinterpretation and overestimation of feature importance before applying XML. This study highlights XML's effectiveness in developing simplified yet highly accurate machine learning models by clarifying feature roles, thereby reducing computational costs for feature acquisition and enhancing model trustworthiness for materials discovery.

Introduction

The rapid advancement of materials informatics has been driven by machine learning (ML), enabling significant improvements in predicting the properties of materials and accelerating their discovery. Nonlinear ML models, such as support vector machines^{1–3} and neural networks,⁴ offer superior predictive performance compared to linear models, and have thus gained popularity. However, the black-box nature of such models limits their interpretability and explainability.^{5–7}

To address this challenge, explainable ML (XML), also known as explainable artificial intelligence (XAI), has gained attention. XML enhances the transparency of the model and fosters scientific understanding by revealing relationships among material structures, compositions, and properties. The use of XML is motivated by the following factors: (i) Understanding the decision-making mechanisms of ML models is essential for building reliable predictive models. (ii) Interpretability aids in debugging unexpected predictions and abnormalities. (iii) XML enables the identification of key predictive features through feature importance analysis, facilitating the reduction of feature preparation costs by eliminating unnecessary features. Notably, XML methods enable nonlinear ML models to explain themselves in an interpretable manner through feature importance metrics, analogous to how linear models use coefficient values to indicate feature significance.

The band gap (E_g) is a critical property that determines the electrical conductivity of a material and its suitability for electronic and optoelectronic applications. Although density functional theory $(DFT)^8$ provides a straightforward approach for estimating the band gap of materials, such predictions are often significantly underestimated. Methods employing hybrid functionals and GW-level calculations offer improved accuracy, albeit at a high computational cost. In particular, the band gap predicted using GW-level calculations have much higher fidelity with the experimental values compared to those predicted using hybrid functionals, but the computational cost of the former is substantially greater, severely limiting the accessible size of the dataset. Consequently, ML models have become indispensable for the efficient prediction of accurate band gap values in materials discovery. Lee *et al.* developed ML models, including support vector regression $(SVR)^{1-3}$, for predicting band gap at the G_0W_0 -level (E_g^{GW}) . Their approach incorporated compound-level features derived from DFT calculations alongside elemental features based on the means and standard deviations of constituent element properties. When utilizing only the band gap computed via generalized gradient approximation using the Perdew–Burke–Ernzerhof (PBE) exchange-correlation functional $(E_g^{PBE})^{12}$ as a single feature, the model achieved a root mean square error (RMSE) of 0.60 eV on the test dataset. By integrating 17 additional features, the accuracy of the optimized model was improved, where the RMSE was reduced to 0.24 eV. However, the contributions of these 17 features to the predictive performance of the model remain insufficiently explored.

Some features may have a negligible impact because their roles overlap owing to strong correlations among the features, or because they do not substantially contribute to accurately predicting the intended prediction objective. Reducing the number of input features could decrease the computational cost of feature preparation and improve the model generalization by mitigating overfitting, which is particularly important for accurate prediction of out-of-domain (OOD) data. Therefore, enhancing the interpretability of such ML models is essential for gaining deeper insights into materials design. Identifying the key predictive features and simplifying the model can reduce the complexity while maintaining high accuracy.

XML methods have been increasingly applied to band gap predictive models in recent studies. Obada $et\ al.^{13}$ employed XML in the analysis of models for predicting band gap for 199 ABX_3 perovskites using element-specific features. However, their analysis was confined to the perovskite family, limiting generalization to broader chemistries. Choubisa $et\ al.^{14}$ introduced the Deep Adaptive Regressive Weighted Intelligent Network, integrating an ML surrogate model, an evolutionary algorithm-based search method, and an interpretable design rule for materials with direct band gap. To enhance the interpretability of the model, they employed Spearman's rank correlation coefficient (r_s) and permutation feature importance (PFI). However, their applications also largely focused on perovskite-like semiconductors, again restricting the material domain. Zhang $et\ al.^{16}$ proposed an interpretable Δ-ML model that correlates the band gap values obtained with the Heyd–Scuseria–Ernzerhof (HSE) hybrid functional and the PBE functional for two-dimensional materials, utilizing the sure independence screening and sparsifying operator (SISSO) algorithm. Shi $et\ al.^{18}$ applied XML techniques, including SHapley Additive exPlanations (SHAP) and SISSO, to models for predicting the thermodynamic stability and band gap computed using the HSE functional for Janus III–IV van der Waals heterostructures. Both of these studies demonstrate the utility of XML in 2D contexts. Nevertheless, the scope of both studies is confined to layered materials rather than bulk inorganic compounds. The abovementioned studies demonstrate the value of XML but are generally restricted to narrow material classes. In addition, these studies did not cross-check the feature importance using multiple XML methods, for example, by combining PFI and SHAP.

Jihad *et al.*²⁰ also proposed a compact five-feature model for correcting $E_{\rm g}^{\rm PBE}$ to $E_{\rm g}^{\rm GW}$ from the same dataset used herein, but their feature selection was based on physics-guided reasoning and manual correlation control rather than XML-based ranking. Therefore, an XML framework applicable to more generalized and diverse datasets is clearly needed.

In this study, we address this need by applying XML to a nonlinear SVR model for predicting $E_{\rm g}^{\rm GW}$ for OOD inorganic materials as well as in-domain systems, including binary and ternary compounds. SVR¹⁻³ is chosen after benchmarking against interpretable linear models such as the ordinary least-square and least absolute shrinkage and selection operator (LASSO)²¹ regressions, as the former consistently achieved higher accuracy and continued to improve with larger training data.¹¹ The strong predictive ability of the selected model makes it a particularly suitable baseline for demonstrating the value of XML, despite its lack of interpretability. The XML methods, PFI¹⁵ and SHAP¹⁹, are systematically combined to guide feature ranking and selection, and the consistency of the feature importance rankings is compared by cross-checking the two methods to ensure reliability. Important features are then identified based on these XML analyses, retaining only those with consistently high importance across both metrics. The derived feature importances are also cross-checked against the coefficient magnitudes obtained from the interpretable LASSO regression. Because highly correlated features can distort importance estimation using XML, such features are eliminated prior to the XML analysis. The effect of this approach is explicitly demonstrated in practical examples in the present study. Through statistical validation and subsampling, the predictive performance and generalization ability of the reduced-feature models are quantitatively evaluated against those of the pristine model using OOD data. Taken together, these steps form a simple and reproducible framework for constructing compact yet interpretable predictive models.

Methods

Band gap predictive model

This study revisits the predictive model proposed by Lee $et~al.^{11}$ for estimating $E_{\rm g}^{\rm GW}$ for 270 binary and ternary inorganic compounds. The pristine model employed SVR $^{1-3}$ with 18 input features $(x_j).^{22}$ Fourteen features are derived from the mean (\bar{x}) and standard deviation $(\sigma(x))$ of the elemental properties, including the absolute oxidation number (|n|), atomic number (Z), period in the periodic table (p), atomic mass (m), van der Waals radius (r), electronegativity (χ) , and ionization energy (I). Notably, these features do not require DFT calculations. Compound-specific properties obtained from DFT calculations are also incorporated, including $E_{\rm g}^{\rm PBE}$, the bandgap computed using the modified Becke–Johnson exchange-correlation functional $(E_{\rm g}^{\rm mBJ}),^{23}$ volume per atom (V), and cohesive energy $(E_{\rm coh})$.

The dataset is split into 75% for training and validation and 25% for testing. For the SVR, a radial basis function kernel is

The dataset is split into 75% for training and validation and 25% for testing. For the SVR, a radial basis function kernel is employed. The hyperparameters are optimized via grid search with ten-fold cross-validation over the following ranges: $C \in \{10^{-5}, 10^{-4}, \dots, 10^4\}$, $\gamma \in \{10^{-6}, 10^{-5}, \dots, 10^5\}$, and $\varepsilon \in \{0.001, 0.005, 0.01\}$. The optimal hyperparameters are determined separately for each training and validation split and subsequently used to train the final SVR model. Predictions are conducted over 20 iterations, with randomized training, validation, and test sets for each attempt. To determine the reproducibility, the random seeds are set to 0–19. Before introduction into the model, all features are standardized via Z–score normalization using

the StandardScaler implemented in the Python Scikit-learn library.²⁴ The entire process is implemented in the same library.

In this study, the feature dimensionality of the pristine model is reduced through a two-step process. First, all feature pairs are subjected to correlation analysis and one feature is removed from each pair exhibiting strong correlation. Second, feature importance is assessed using PFI and SHAP, retaining only the most significant features. The impact of this reduced-feature set on the predictive performance of the model is then evaluated.

For comparison, LASSO regression, which can perform both shrinkage and embedded feature selection based on L_1 penalty, is also employed as an interpretable linear baseline. This method is trained using the same standardized features and 20 randomized train/validation/test splits as used for SVR. The regularization strength α is optimized by 10-fold cross-validation using 200 logarithmically spaced values between 10^{-6} and 10^2 , and the maximum iteration number is set to 100,000 to ensure convergence.

The dataset used to construct the model consists of 270 binary and ternary compounds containing sp— or fully occupied d—metal elements, referred to as the in-domain dataset. An OOD dataset comprising 30 materials is also prepared. Unlike the in-domain dataset, the OOD dataset includes compounds with transition metals or quaternary/pentanary elements. The degree of distributional shift between the in-domain and OOD datasets is evaluated by applying the Kolmogorov–Smirnov test to the feature distributions, as shown in Supplementary Fig. S1. Among the 18 features, 11 exhibit statistically significant differences (p < 0.01, 99% confidence level), confirming that the OOD dataset lies outside the feature distribution of the in-domain dataset. This OOD dataset is used to test the hypothesis that an XML-guided compact model would achieve better generalization for chemically distinct systems than the more complex pristine model, which may be overfitted to the in-domain distribution. The materials are selected from the Materials Project Database²⁵ through arbitrary sampling, ensuring computational feasibility under the following constraints: fewer than 20 atoms per unit cell and no significant challenges in electronic iteration convergence. Feature generation and prediction objectives are determined using first-principles calculations under the same computational conditions as described by Lee *et al.*¹¹ The list and properties of the OOD dataset are provided in Supplementary Table S1.

Permutation feature importance (PFI)

PFI¹⁵ is a global XML method used to quantify the contribution of a feature to the predictions of the model. It assesses the feature importance by independently shuffling each feature and measuring the impact on the predictive performance of the model. The PFI score for the j-th feature is defined as the increase in the predictive error of the model when the feature is permuted, relative to the error of the original model. In this study, the PFI scores are computed by shuffling features in the test dataset and evaluating the corresponding increase in the RMSE.

SHapley Additive exPlanation (SHAP)

SHAP¹⁹ is an XML method that explains the prediction of individual samples by attributing the model's output to different features. Rooted in cooperative game theory's principle of fair distribution, SHAP assigns an importance value to each feature, quantifying its contribution to a specific prediction. Conceptually, SHAP values average a feature's marginal contribution over all possible feature coalitions.

SHAP represents predictions via an additive explanation model:

$$g(x') = \phi_0 + \sum_{j=1}^{n_x} \phi_j x'_j, \qquad x' \in \{0, 1\}^{n_x}, \tag{1}$$

where n_x is the number of input features in the model being explained, x' is a binary coalition vector indicating feature presence $(x'_j = 1)$ or absence $(x'_j = 0)$, ϕ_j is the SHAP value of feature j, and ϕ_0 is the base value, corresponding to the expected prediction over the background data. For a coalition x', features with $x'_j = 0$ are marginalized over the background distribution, while those with $x'_j = 1$ are conditioned on their observed values; aggregating over all coalitions (all $x'_j = 1$) yields SHAP values that satisfy local accuracy as follows:

$$\hat{f}(x) = g(\mathbf{1}) = \phi_0 + \sum_{j=1}^{n_x} \phi_j. \tag{2}$$

The SHAP value for the *j*-th feature is defined as

$$\phi_{j} = \sum_{S \subseteq F \setminus \{j\}} \frac{|S|! \left(|F| - |S| - 1\right)!}{|F|!} \left[\hat{f}_{S \cup \{j\}} \left(x_{S \cup \{j\}} \right) - \hat{f}_{S} \left(x_{S} \right) \right], \quad \text{with } |F| = n_{x},$$
(3)

where F is the full set of features considered at this stage, and the sum runs over all subsets $S \subseteq F \setminus \{j\}$, excluding j-th feature. Here, $\hat{f}_S(x_S)$ denotes the model prediction when only the features in S are present and all other features are integrated out using the background distribution, and $\hat{f}_{S \cup \{j\}}(x_{S \cup \{j\}})$ is defined analogously.

SHAP can provide both local and global explanations. In this study, SHAP importance, a global explanation approach, is used. It represents feature importance by averaging the absolute SHAP values across all samples. SHAP values are computed using the model-agnostic KernelExplainer implemented in the Python SHAP library²⁶ with the standardized training set as the background dataset for each split. For each test sample, SHAP values are approximated by sampling up to 100 feature coalitions based on the Shapley kernel weighting scheme when estimating marginal contributions. This setting is chosen to balance computational efficiency with the stability of the SHAP estimates.

Significance test

To assess whether one predictive model achieves a statistically significant improvement in the accuracy over another, the per-trial RMSE values are analyzed using paired *t*-tests. In each trial, the same random seed is used for data splitting, and the resulting RMSE values of the two models are compared in pairs. A 99% confidence level is adopted: If the *p*-value exceeds 0.01, the two models are regarded as not significantly different, whereas a *p* value less than 0.01 indicates that the predictive performance of one model is statistically superior. This procedure ensures that observed performance differences are evaluated for consistency across the 20 randomized trials rather than being attributed to chance.

Results

Feature correlations

Before applying XML methods, the feature correlations were analyzed. Supplementary Fig. S2 presents the correlation matrix of all features. Pearson's correlation coefficient (r_p) is an indicator of linear correlations based on actual values, whereas Spearman's rank correlation coefficient (r_s) is used to evaluate monotonic relationships using ranked data points instead of actual values. To mitigate redundancy, only one feature was retained from each highly correlated pair, defined as those with r_s or r_p exceeding 0.8. This threshold was chosen because correlations above 0.8 indicate very strong redundancy, and lowering the cutoff led to a rapid increase in the prediction error (see Supplementary Table S2). Retention decisions were made by reconstructing the predictive models while excluding each feature individually. If the exclusion of a feature results in a statistically significant increase in the prediction error, the feature is retained and its correlated counterpart is removed. If neither exclusion causes a significant increase in the error, the feature with the lower correlation to the prediction objective (E_g^{GW}) is removed. Consequently, seven features were eliminated from the original 18-feature set in the order: \bar{m} , $\sigma(Z)$, E_g^{mBJ} , \bar{p} , \bar{I} , $\sigma(I)$, and V. The detailed elimination order is presented in Supplementary Table S2. The removal of these features improves the consistency in the XML analysis, as further expounded in the Discussion section.

XML results and important feature selection

The reduced 11-feature set was used to construct a predictive model under the same conditions used for the original 18-feature set. XML methods, PFI and SHAP, were then applied to assess the feature importance.

Figure 1 (left bar) presents the PFI scores for the prediction of $E_{\rm g}^{\rm GW}$ using the SVR model. Among the features, $E_{\rm g}^{\rm PBE}$ exhibited the highest PFI score (2.91 eV), indicating its dominant influence on the predictions. The next most important features— $\bar{\chi}$, $\sigma(\chi)$, and $|\bar{n}|$ —had PFI scores ranging from 0.28 to 0.35 eV. In contrast, the remaining features, beginning with $\sigma(p)$, had relatively low PFI scores (0.03–0.08 eV), suggesting minimal impact on the performance of the model. A higher PFI score indicates a greater contribution to the predictive accuracy, whereas near-zero scores suggest that variations in the values of the feature do not significantly affect the predictions, rendering the feature less influential.

Figure 1 (right bar) also presents the SHAP importance scores, which provide a quantitative indicator of the contribution of each feature to the prediction of $E_{\rm g}^{\rm GW}$ using the SVR model with the 11-feature set. Among the features, $E_{\rm g}^{\rm PBE}$ had the highest SHAP importance score (1.85 eV), followed by $\sigma(\chi)$, $\bar{\chi}$, and $|\bar{n}|$ with values ranging from 0.23 to 0.28 eV. The remaining features, starting from $\sigma(p)$, exhibited lower SHAP importance scores (0.01–0.07 eV). These findings align with the results of the PFI analysis.

To further investigate the directional influence of the features on the predictions, r_p was analyzed for the feature values and SHAP values using the test dataset. A positive r_p indicates that an increase in the feature contributes to an increase in the SHAP value, whereas a negative r_p suggests the opposite effect. The five most influential features (E_g^{PBE} , $\sigma(\chi)$, $\bar{\chi}$, $|\bar{n}|$, and $\sigma(p)$) consistently retained the same r_p sign across 20 different data selections. Specifically, increases in E_g^{PBE} , $\sigma(\chi)$, and $\bar{\chi}$ led to higher SHAP values, whereas increases in $|\bar{n}|$ and $\sigma(p)$ decreased the SHAP values. The remaining features exhibited inconsistent r_p signs and have relatively lower SHAP-importance scores. This trend is further visualized in Supplementary Fig. S3, which includes beeswarm plots illustrating the relationship between the features and SHAP values.

To systematically assess the impact of feature selection, the feature importance scores from both XML methods were averaged and the features were ranked in descending order of importance, as shown on the horizontal axes of Fig. 1. Based on these rankings, " n_x -feature sets" were constructed, where n_x represents the number of selected features ($n_x = 2$ to 11). Predictive models were then developed using these progressively refined feature sets, in accordance with their XML-derived importance rankings.

Dependence of reduced-feature set on predictive performance

Figure 2a shows the relationship between the prediction error (RMSE) of the test dataset and the number of selected features (n_x) ranked by the XML importance. Other error-related metrics are summarized in Supplementary Table S3 and Fig. S4. A lower RMSE indicates better predictive performance. After removing the seven highly correlated features, the predictive performance of the model employing the 11-feature set remained comparable to that of the pristine model. As n_x decreased from 11 to 5, the model maintained stable performance, with the RMSE of the test dataset ranging between 0.253 and 0.266 eV. However, when $n_x \le 4$, the predictive performance declined and the RMSE increased beyond this range, indicating that further feature reduction negatively impacts the performance of the model.

The prediction error of the training dataset gradually increased as n_x decreased, as shown in Supplementary Fig. S5. A smaller n_x corresponds to a simpler predictive model. The generalization gap, defined as the difference between the training and test dataset errors, provides an indicator of overfitting and the robustness of the model, where a smaller gap suggests more consistent performance between the training and unseen data. Notably, the generalization gap was smallest when $n_x = 2$, although the corresponding RMSE values were higher than those obtained with models using more features. When n_x increased beyond 2, the generalization gap tended to widen, as illustrated in Fig. 2a.

Thus far, the predictive performance of the model has been evaluated using the in-domain data. To assess the performance in evaluating OOD data, the dependence of the prediction error on n_x was also examined. Figure 2b shows the relationship between n_x and the prediction error for the OOD dataset based on the features selected using the XML importance. The RMSE of the pristine model was 0.461 eV for the OOD dataset, which was significantly higher than the RMSE of 0.247 eV for the in-domain dataset. However, predictive models using n_x -feature sets ($n_x = 4$ to 8) outperformed the pristine model in predicting the OOD data. Notably, for $n_x = 5$ to 7, the RMSE ranged from 0.331 to 0.344 eV, representing a reduction exceeding 0.1 eV compared to that of the pristine model. For $n_x = 5$, 6, and 7, the 99% confidence intervals of the RMSE differences relative to those of the pristine models were all negative, with ranges of (-0.156, -0.085), (-0.154, -0.081), and (-0.162, -0.099), respectively. The corresponding p-values were all less than 10^{-8} , confirming that the compact models consistently and significantly outperformed the pristine model in predicting the OOD data.

To further examine the robustness of the model with respect to the size of the OOD dataset, subsampling analyses with 20, 25, and 30 OOD compounds were performed for the compact models with $n_x = 5$ to 7 and for the pristine model. The results shown in Supplementary Fig. S6 confirmed that the predictive performance of the models remained stable regardless of the sample size. Although the size of the OOD dataset is limited to 30 compounds, the statistical and subsampling analyses confirm that this number is sufficient to robustly demonstrate the superiority of the compact models.

The predictive deviations (\bar{d}) based on the selected data were also examined. The predictive deviation for the *i*-th sample (d_i) was calculated as the standard deviation across 20 different predictions:

$$d_i = \sqrt{\frac{1}{N_c} \sum_{c=1}^{N_c} (\hat{y}_{c,i} - \bar{y}_i)^2}$$
 (4)

where c represents the attempt number for data selection, N_c is the total number of attempts, $\hat{y}_{c,i}$ is the predicted value for the i-th sample in the c-th attempt, and \bar{y}_i is the mean predicted value for the i-th sample. The predictive deviations were then averaged across the 30 OOD data points. The models employing the n_x -feature set exhibited smaller predictive deviations than the pristine model (0.157 eV). Notably, for $n_x = 2$ to 7, the predictive deviations remained below 0.1 eV.

For $n_x = 3$ to 10, random feature sets were used for comparison. To prevent excessively high prediction errors, each random feature set included E_g^{PBE} . In both the in-domain and OOD datasets, most random feature sets resulted in higher prediction errors than the n_x -feature sets selected based on the XML importance scores. Although some random feature sets yielded low RMSE values for the in-domain dataset (< 0.30 eV), the corresponding RMSE values for the OOD dataset exceeded 0.46 eV, as shown by the green circles in Fig. 2b. This suggests that these models are overfitted to the in-domain dataset and lack generalization capability for the OOD dataset.

For comparison, an interpretable linear regression baseline using LASSO was also examined. Similar to SVR, the seven highly correlated features were first removed, and the coefficient magnitudes at $n_x = 11$ were used as a measure of the importance for ranking the features. Models with $n_x = 2$ to 11 features were then constructed in descending order of importance. As shown in Supplementary Fig. S7, although the ranking sequence differed slightly, the top five most important features

selected by LASSO were identical to those identified by SVR. The numbers of nonzero (unshrunk) features are summarized in Supplementary Fig. S8. Notably, for $n_x = 2$ to 8, no additional shrinkage occurred, and the input features were retained as nonzero coefficients.

Figure 2 presents a comparison of the predictive performance of the LASSO regression models with that of SVR. Across all n_x , SVR consistently outperformed LASSO for treatment of the in-domain dataset. For the OOD dataset, SVR also achieved lower errors than LASSO for $n_x = 2$ to 8. Similar to SVR, the predictive performance of LASSO improved as the number of features decreased compared to the pristine model, for which the feature count shrank from 18 to only about 17 on average across twenty different trials. However, using the optimal feature count ($n_x = 5$ to 7), the predictive performance of SVR still surpassed that of LASSO by approximately 0.05 eV, confirming the advantageous generalization performance of the former.

Discussion

Insights for feature selection

The proposed framework for selecting important features and reducing the dimensionality based on the XML importance offers several advantages.

First, it simplifies the predictive model, enhancing its interpretability. This reduction in complexity also narrows the generalization gap, improving the model's ability to predict OOD data. Consequently, the predictive model employing only the five most important features outperforms the pristine model in predicting the OOD dataset, while the performance remains comparable to that with the in-domain dataset. Moreover, the models with reduced-feature sets exhibit lower predictive deviations across different data selections, as shown in Fig. 2c and Fig. 2d. For reference, the predictive deviations across different data selections for all the feature sets are also presented in Supplementary Fig. S9. A smaller feature set further reduces the cost of data collection and mitigates the risk of unavailable data in practical applications.

This framework provides a systematic approach for determining the optimal n_x . By incrementally adding features based on their XML importance ranks, the predictive performance can be monitored, eliminating the need for evaluating an overwhelming number of feature set combinations.

Number of available combinations of feature sets =
$$\sum_{n_x=1}^{N_x} C(N_x, n_x),$$
 (5)

where N_x is the total number of features and C represents the combination function. For $N_x = 18$, equation (5) results in over 410,000 possible feature sets. In this study, 80 random feature sets were evaluated for $n_x = 3$ to 10. The performance of most predictive models employing random feature sets is inferior to that of models constructed with feature sets selected based on the XML importance, for both in-domain and OOD datasets. Some random feature sets exhibit low in-domain errors but perform poorly in predicting OOD data (green circles in Fig. 2), underscoring that XML-guided selection does not merely identify any feature subset that appears effective in-domain, but rather ensures robust generalization for chemically distinct systems.

Given the comparable prediction error for the in-domain dataset (0.254 eV) and the reduced generalization gap compared to models with more features and the pristine model, the 5-feature set suggested by XML importance scores proves to be both sufficient and robust for predictive modeling. Although the generalization gap is smallest for the model with 2-feature set, its RMSE value is considerably higher than those of models with more features, making them less practical for prediction. In contrast, the model with 5-feature set maintains a low RMSE and robust generalization, thus providing the most suitable balance between accuracy and simplicity. Moreover, this feature set achieves a sufficiently low prediction error for the OOD dataset (0.341 eV) with smaller predictive deviations compared to models with more features and the pristine model.

The 5-feature set consists of E_g^{PBE} , $\sigma(\chi)$, $\bar{\chi}$, $|\bar{n}|$, and $\sigma(p)$. The first three features exhibit positive correlations with the prediction objective E_g^{GW} , whereas the latter two have negative correlations. These correlations align with the signs observed for the features and the corresponding SHAP values. The r_p (r_s) values for the features and E_g^{GW} , ordered on the basis of the XML importance scores, are as follows: 0.98 (0.98), 0.80 (0.81), 0.57 (0.48), -0.59 (-0.63), and -0.11 (-0.07).

Although the XML importance scores of $\bar{\chi}$ and $|\bar{n}|$ are similar to that of $\sigma(\chi)$, their correlations with the prediction objective are lower. Interestingly, $\sigma(p)$, which does not show a significant correlation with the prediction objective, still contributes to the improved predictive performance. This contribution is evident from the differences in the prediction errors for the models with the *4-feature* and *5-feature sets*, as shown in Fig. 2. A plausible explanation is that $\sigma(p)$ reflects the variation of the constituent elements across different periods of the periodic table, which may act as a proxy for underlying chemical diversity. Such diversity can influence the bonding heterogeneity, structural complexity, or ionicity, factors that are not directly captured by other features. While speculative, this suggests that $\sigma(p)$ provides complementary information about material diversity, enabling better generalization. This observation suggests that XML does not merely recover physically intuitive features such as the $E_{\rm g}^{\rm PBE}$, electronegativity, and oxidation number, but can also highlight less obvious features that yield new insights into

the behavior of materials. It also confirms that the XML importance provides a more accurate and intuitive explanation of the feature contributions, which may not be fully captured by simple correlations between features and the prediction objective.

The XML-based feature ranking from the SVR model was further compared with the coefficient magnitudes obtained from LASSO using the same 11-feature set (see Fig. 1 and Supplementary Fig. S7). Although the exact ranking sequence differs slightly, the top five features identified by LASSO coincide with those obtained by the XML-guided SVR analysis. When these five features were manually used as the input features in LASSO, the predictive performance remained comparable to that of the pristine model for the in-domain dataset and is even improved for the OOD dataset, confirming that the selected features are robust across different regression frameworks. Moreover, although LASSO has built-in shrinkage capability, no additional shrinkage was obtained when fewer than nine input features were used (see Supplementary Fig. S8), also highlighting the usefulness and necessity of feature-selection methods based on the feature importance for different regression frameworks.

The selected feature set based on the XML importance aligns well with the feature sets constructed using scientific insights. Jihad *et al.*²⁰ proposed a reduced set of five features based on Coulombic interactions, where Gaussian regression was used to predict E_g^{GW} from the same dataset. Their feature set included E_g^{PBE} , $|\bar{n}|$, $\bar{\chi}$, $\sigma(\chi)$, and volume^{1/3}. Notably, the first four features overlap with those in the *5-feature set* suggested by the XML importance in this study. When the feature set proposed by Jihad *et al.*²⁰ was applied to the in-domain and OOD datasets using the SVR model developed in this study, the resulting RMSE values were 0.280 eV and 0.345 eV, respectively. These values are slightly higher than the RMSE obtained with the *5-feature set* identified in this study, further demonstrating the effectiveness of XML-based feature selection.

Correlated feature elimination prior to XML analysis

The rationale for removing strongly correlated features before performing XML analysis is discussed here. Figure 3a presents the top five features with the highest SHAP importance scores for the pristine model using the full 18-feature set. A complete list of the SHAP importance scores for all 18 features is provided in Supplementary Fig. S10. Notably, the ranking of important features differs from that obtained with the 11-feature set. Specifically, $\sigma(Z)$ and $\sigma(m)$ exhibit significantly high SHAP importance scores. As shown in Supplementary Fig. S2, $\sigma(m)$ has a negative correlation with the prediction objective E_g^{GW} . Nevertheless, its SHAP values are positively correlated with $\sigma(m)$ itself. This contradiction suggests that the presence of highly correlated features may distort the SHAP importance scores. Figure 3b illustrates the relationship between $\sigma(Z)$ and $\sigma(m)$, two features identified as important through XML analysis. The correlation coefficient for the relationship between these features is 0.995, indicating an extremely strong positive correlation. Figure 3c presents the distribution of the SHAP values for these two features. Despite their strong correlation, their SHAP values exhibit opposite signs. Such compensating behavior was not limited to the nonlinear SVR model. A similar phenomenon was also observed in the full 18-feature LASSO model, as shown in Supplementary Fig. S11. Even with shrinkage regularization, the number of nonzero coefficients decreased only marginally (to approximately 17). Mirroring the behavior observed in the SHAP analysis of the SVR model, the coefficients of $\sigma(Z)$ and $\sigma(m)$ exhibited large magnitudes with opposite signs.

When the SHAP importance of $\sigma(m)$ was recalculated using the 17-feature set (excluding $\sigma(Z)$), its rank dropped from 3rd to 15th, and its importance score decreased from 0.60 to 0.02, as shown in Supplementary Fig. S10. A consistent trend was observed in the LASSO analysis: when $\sigma(Z)$ was excluded from the input feature set, the coefficient of $\sigma(m)$ became very small and negligible, as shown in Supplementary Fig. S11. This result suggests that neither feature is inherently crucial to the predictive performance of the model; rather, their apparent importance is overestimated when both are included, as they counterbalance each other's impact on the predicted output. More generally, this counterbalancing effect serves as a methodological lesson: highly correlated features can artificially inflate each other's importance scores in XML analyses, and their removal is essential for obtaining a true and reliable picture of feature contributions. SHAP analysis assumes feature independence. However, when applied in materials design, achieving complete independence is challenging because commonly used physics- and chemistry-based features often exhibit some degree of correlation. Therefore, strongly correlated features should be removed before performing XML analysis and regression modeling, even when using linear shrinkage methods such as LASSO, to ensure accurate and reliable results.

Conclusion

In this study, PFI and SHAP were systematically combined and applied to a nonlinear SVR predictive model for $E_{\rm g}^{\rm GW}$ to interpret and explain the predictions while identifying key features. These XML methods provided consistent feature-importance rankings, enabling the selection of the most significant features and reducing model complexity. By sequentially adding features based on their importance rankings, the optimal number of features was determined. The feature importance rankings were further cross-checked against the coefficient magnitudes obtained from interpretable LASSO regression, confirming consistency between the methods. To prevent distortion of the importance estimation, strongly correlated features were removed prior to XML analysis, and the necessity of this preprocessing step was explicitly demonstrated through a practical example.

The selected *5-feature set*, based on XML importance scores, demonstrated comparable predictive performance with a smaller generalization gap for the in-domain dataset and achieved superior predictive performance for the OOD dataset compared to the more complex pristine model. The proposed XML-guided feature selection framework offers a systematic, reproducible, and effective approach for constructing compact and interpretable predictive models, which can be extended to other materials informatics applications.

References

- **1.** Boser, B. E., Guyon, I. M. & Vapnik, V. N. A training algorithm for optimal margin classifiers. *Proc. Fifth ann. Work. comput. Learn. Theor.* 144–152 (1992).
- 2. Hearst, M. A., Dumais, S. T., Osuna, E., Platt, J. & Schölkopf, B. Support vector machines. *IEEE Intell. Syst. Their Appl.* 13, 18–28 (1998).
- 3. Smola, A. J. & Schölkopf, B. A tutorial on support vector regression. Stat. Comput. 14, 199–222 (2004).
- **4.** LeCun, Y., Bengio, Y. & Hinton, G. Deep learning. *Nature* **521**, 436–444 (2015).
- 5. Molnar, C. Interpretable Machine Learning (2022), 2nd edn.
- 6. Zhong, X. et al. Explainable machine learning in materials science. npj Comput. Mater. 8, 204 (2022).
- **7.** Oviedo, F., Ferres, J. L., Buonassisi, T. & Butler, K. T. Interpretable and explainable machine learning for materials science and chemistry. *Acc. Mater. Res.* **3**, 597–607 (2022).
- **8.** Kohn, W. & Sham, L. J. Self-consistent equations including exchange and correlation effects. *Phys. Rev.* **140**, A1133–A1138 (1965).
- **9.** Heyd, J., Scuseria, G. E. & Ernzerhof, M. Hybrid functionals based on a screened Coulomb potential. *J. Chem. Phys.* **118**, 8207–8215 (2003).
- **10.** Fuchs, F., Furthmüller, J., Bechstedt, F., Shishkin, M. & Kresse, G. Quasiparticle band structure based on a generalized Kohn-Sham scheme. *Phys. Rev. B* **76**, 115109 (2007).
- 11. Lee, J., Seko, A., Shitara, K., Nakayama, K. & Tanaka, I. Prediction model of band gap for inorganic compounds by combination of density functional theory calculations and machine learning techniques. *Phys. Rev. B* 93, 115104 (2016).
- **12.** Perdew, J. P., Burke, K. & Ernzerhof, M. Generalized gradient approximation made simple. *Phys. Rev. Lett.* **77**, 3865–3868 (1996).
- **13.** Obada, D. O. *et al.* Explainable machine learning for predicting the band gaps of ABX₃ perovskites. *Mater. Sci. Semicond. Process.* **161**, 107427 (2023).
- **14.** Choubisa, H. et al. Interpretable discovery of semiconductors with machine learning. npj Comput. Mater. **9**, 117 (2023).
- **15.** Fisher, A., Rudin, C. & Dominici, F. All models are wrong, but many are useful: Learning a variable's importance by studying an entire class of prediction models simultaneously. *J. Mach. Learn. Res.* **20**, 1–81 (2019).
- **16.** Zhang, L. *et al.* Accurate band gap prediction based on an interpretable Δ-machine learning. *Mater. Today Commun.* **33**, 104630 (2022).
- 17. Ouyang, R., Curtarolo, S., Ahmetcik, E., Scheffler, M. & Ghiringhelli, L. M. SISSO: A compressed-sensing method for identifying the best low-dimensional descriptor in an immensity of offered candidates. *Phys. Rev. Mater.* 2, 083802 (2018).
- **18.** Shi, Y. *et al.* Interpretable machine learning for stability and electronic structure prediction of Janus III–VI van der Waals heterostructures. *MGE Adv.* **2**, e76 (2024).
- **19.** Lundberg, S. M. & Lee, S.-I. A unified approach to interpreting model predictions. *Adv. Neural Inf. Process. Syst.* **30** (2017).
- **20.** Jihad, I., Anfa, M. H. S., Alqahtani, S. M. & Alharbi, F. H. DFT-PBE band gap correction using machine learning with a reduced set of features. *Comput. Mater. Sci.* **244**, 113153 (2024).
- **21.** Tibshirani, R. Regression shrinkage and selection via the lasso. *J. Royal Stat. Soc. Ser. B: Stat. Methodol.* **58**, 267–288 (1996).
- 22. GWgap_predictor_data. http://github.com/JoohwiLEE/GWgap_predictor_data. Last Accessed: Nov 22 2023.
- **23.** Tran, F. & Blaha, P. Accurate band gaps of semiconductors and insulators with a semilocal exchange-correlation potential. *Phys. Rev. Lett.* **102**, 226401 (2009).

- 24. Pedregosa, F. et al. Scikit-learn: Machine learning in Python. J. Mach. Learn. Res. 12, 2825–2830 (2011).
- **25.** Jain, A. *et al.* Commentary: The materials project: A materials genome approach to accelerating materials innovation. *Appl. Phys. Lett. Mater.* **1**, 011002 (2013).
- 26. SHAP. http://github.com/shap/shap. Last Accessed: Nov 28 2023.

Data Availability

The in-domain data can be obtained at http://github.com/JoohwiLEE/GWgap_predictor_data. Other raw/processed data can be found in this article.

Acknowledgements

The authors would like to thank Enago (www.enago.jp) for the English language review.

Author Contributions

J. L. primarily performed the simulations and prepared the first manuscript. K. M. designed the project. All authors discussed the results and wrote the manuscript.

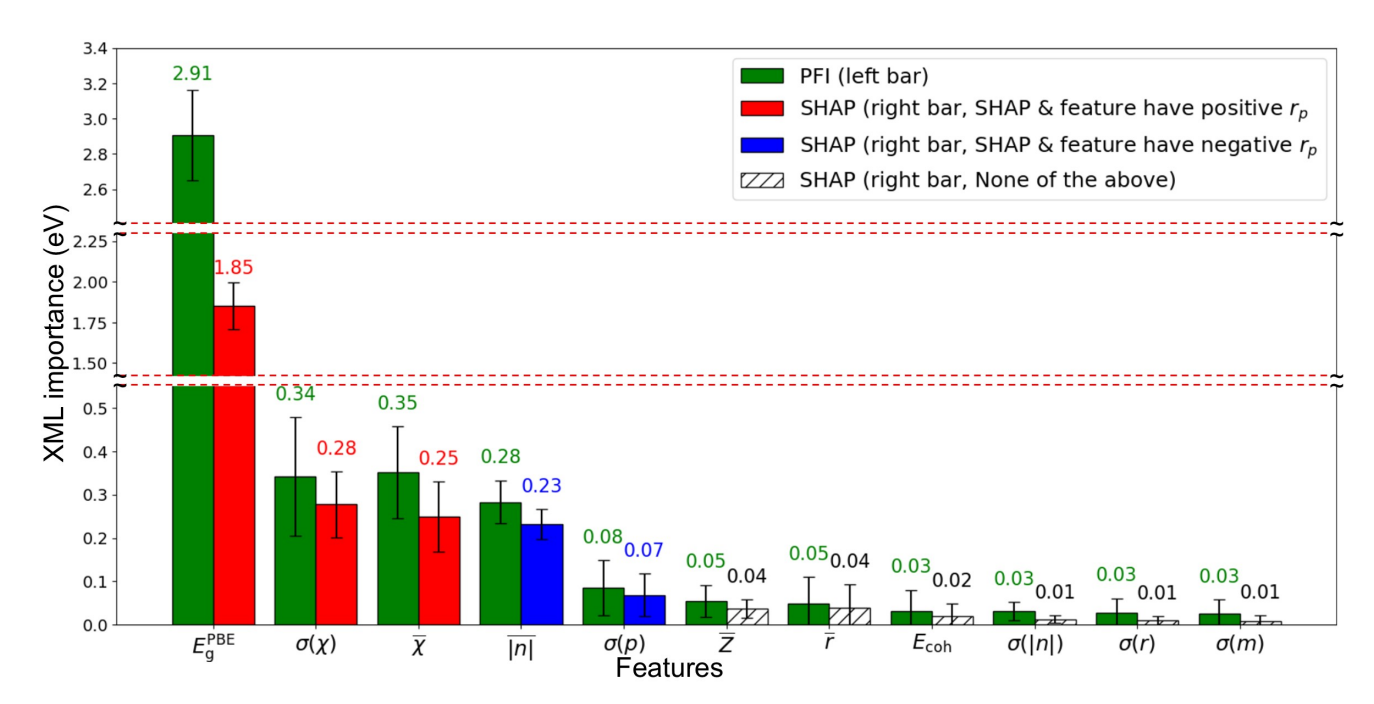


Figure 1. XML importance scores of SVR regression model for predicting $E_{\rm g}^{\rm GW}$ using 11-feature set. For each feature, the paired bars represent the PFI (left bar) and SHAP importance (right bar). The PFI score is calculated as the increase in the RMSE for the analysis using the test dataset when the values of a specific feature are shuffled, where the predictive model is trained using the training dataset. The SHAP importance score is calculated as the mean of the absolute values of the individual SHAP values from the test dataset. If the signs of r_p for the SHAP and predicted values are consistently positive or negative across the predictive models using 20 different data selections, the bars are colored red and blue, respectively. The hatched bars indicate that the signs vary across the predictive models. The error bars represent one standard deviation of the XML importance scores across the predictive models constructed using 20 different data selections. The features are displayed in descending order based on the average PFI and SHAP importance scores.

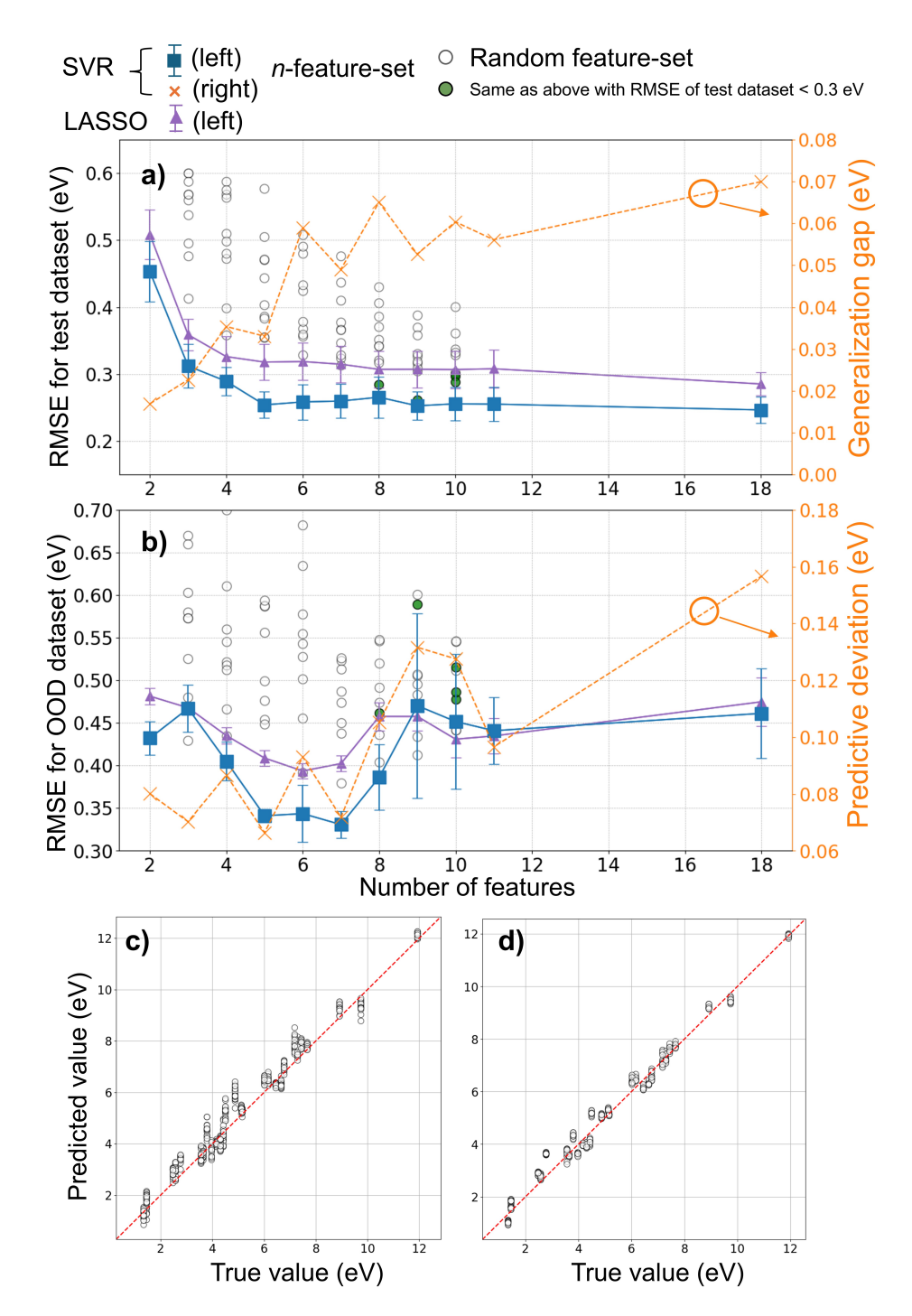


Figure 2. SVR regression models for $E_{\rm g}^{\rm GW}$ prediction using various feature sets. (a) Dependence of the RMSE for the test in-domain dataset (cyan rectangles) and generalization gap (orange \times , right vertical axis) on the number of features selected based on XML importance scores. (b) Dependence of the RMSE for the OOD dataset (cyan rectangles) and the predicted value deviations (orange \times , right vertical axis) on the number of features selected based on the XML importance scores using 20 different data selections. The values at $n_x = 18$ correspond to the pristine model. Error bars indicate one standard deviation across the predictive models using 20 different data selections. For $n_x = 3$ to 10, 10 predictive models with random feature sets, including $E_{\rm g}^{\rm PBE}$, were constructed, represented by empty circles. In addition, models with low RMSE values for the in-domain test dataset (<0.30 eV) are represented by green circles in panels (a) and (b). Values exceeding the range of the vertical axis are not displayed. LASSO results are also shown for comparison; here the horizontal axis indicates the number of input features, and the feature order for $n_x = 2$ to 11 is determined by ranking the coefficients in the *11-feature* LASSO model by their absolute magnitude. Parity plots for the 30 OOD data points: (c) Pristine model with *18-feature set* and (d) predictive model with *5-feature set*. Each dot represents the predicted values from the predictive models with 20 different data selections. The parity plots for the models with all the other feature sets are displayed in Supplementary Fig. S9.

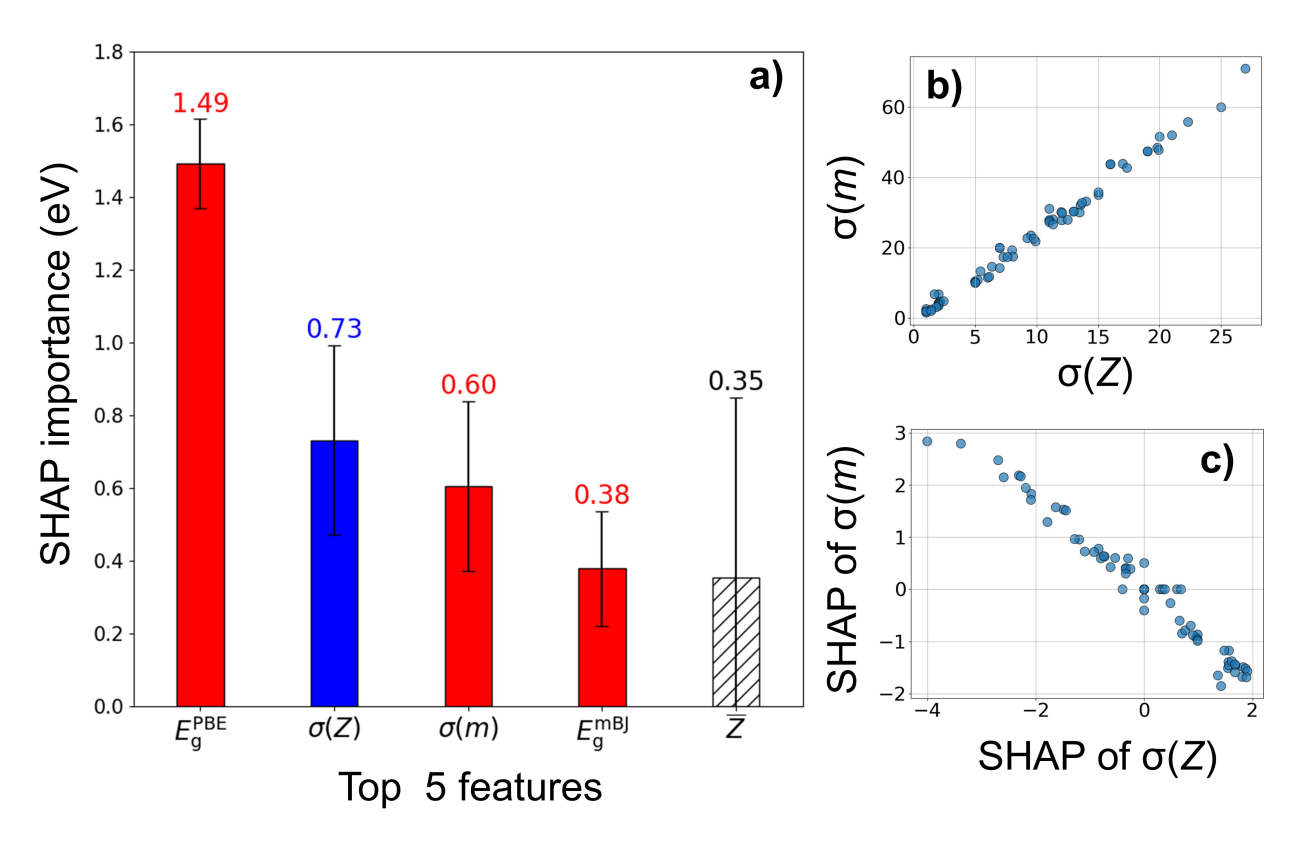


Figure 3. (a) Top five features with SHAP importance scores for SVR regression model for $E_{\rm g}^{\rm GW}$ prediction using 18-feature set. The SHAP importance scores for all 18 features are provided in Supplementary Fig. S10. Detailed information relevant to most options, such as error bars and colors for the bar graph, is presented in Fig. 1. Relationships between (b) $\sigma(Z)$ and $\sigma(m)$, and (c) SHAP values for $\sigma(Z)$ and $\sigma(m)$ of test dataset.

Supplementary Information

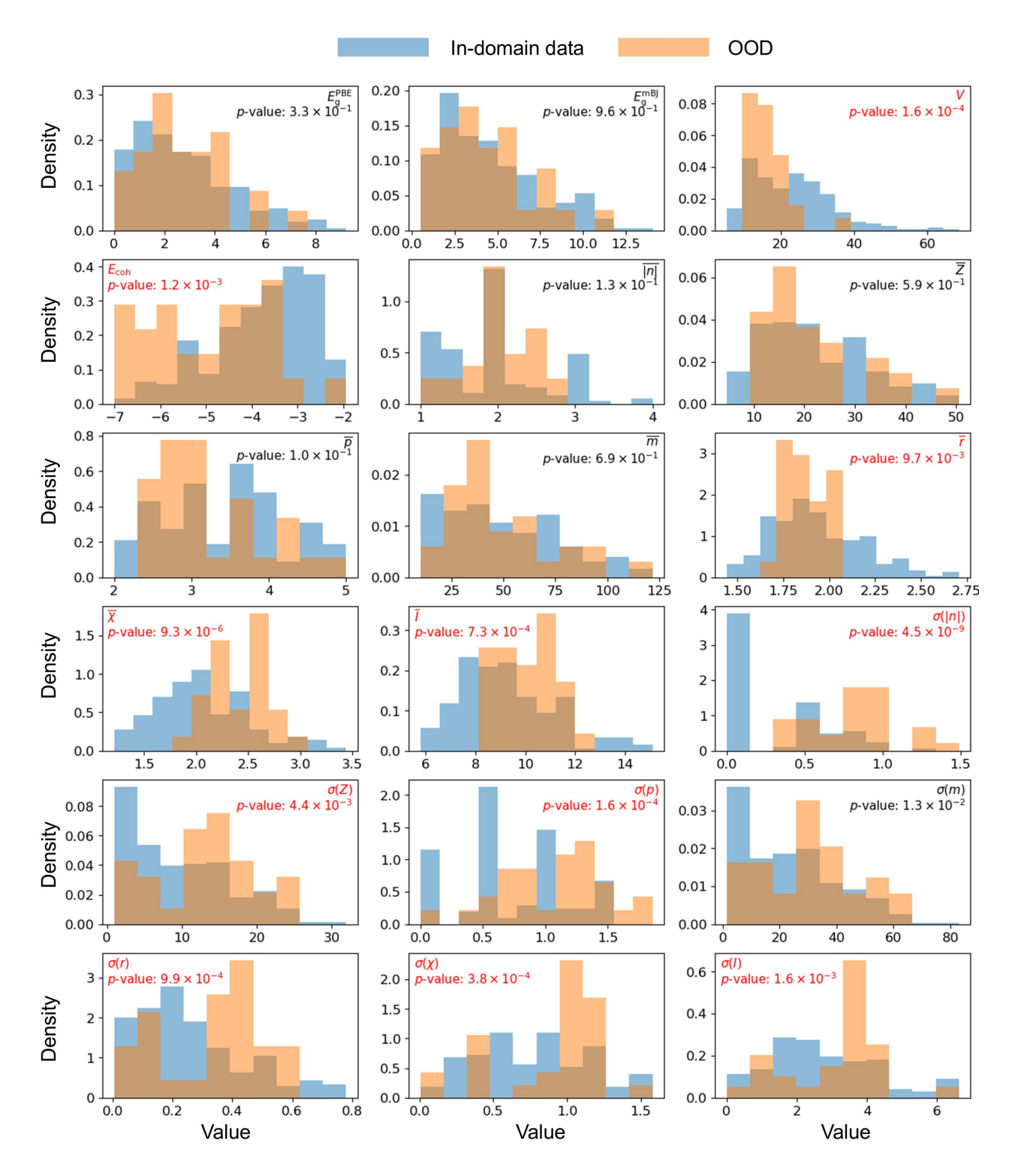


Figure S1. Comparison of in-domain (270 compounds composed of binary and ternary systems) and out-of-domain (OOD) datasets (30 compounds containing transition metals and/or quaternary/pentanary systems) for 18 material features. Each subplot shows the probability density distributions of the corresponding feature for both datasets. The Kolmogorov–Smirnov test is used to determine whether the two distributions originate from the same population. The *p*-value is shown in each panel; values smaller than 0.01, shown in red, indicate that the in-domain and OOD distributions are significantly different at the 99% confidence level.

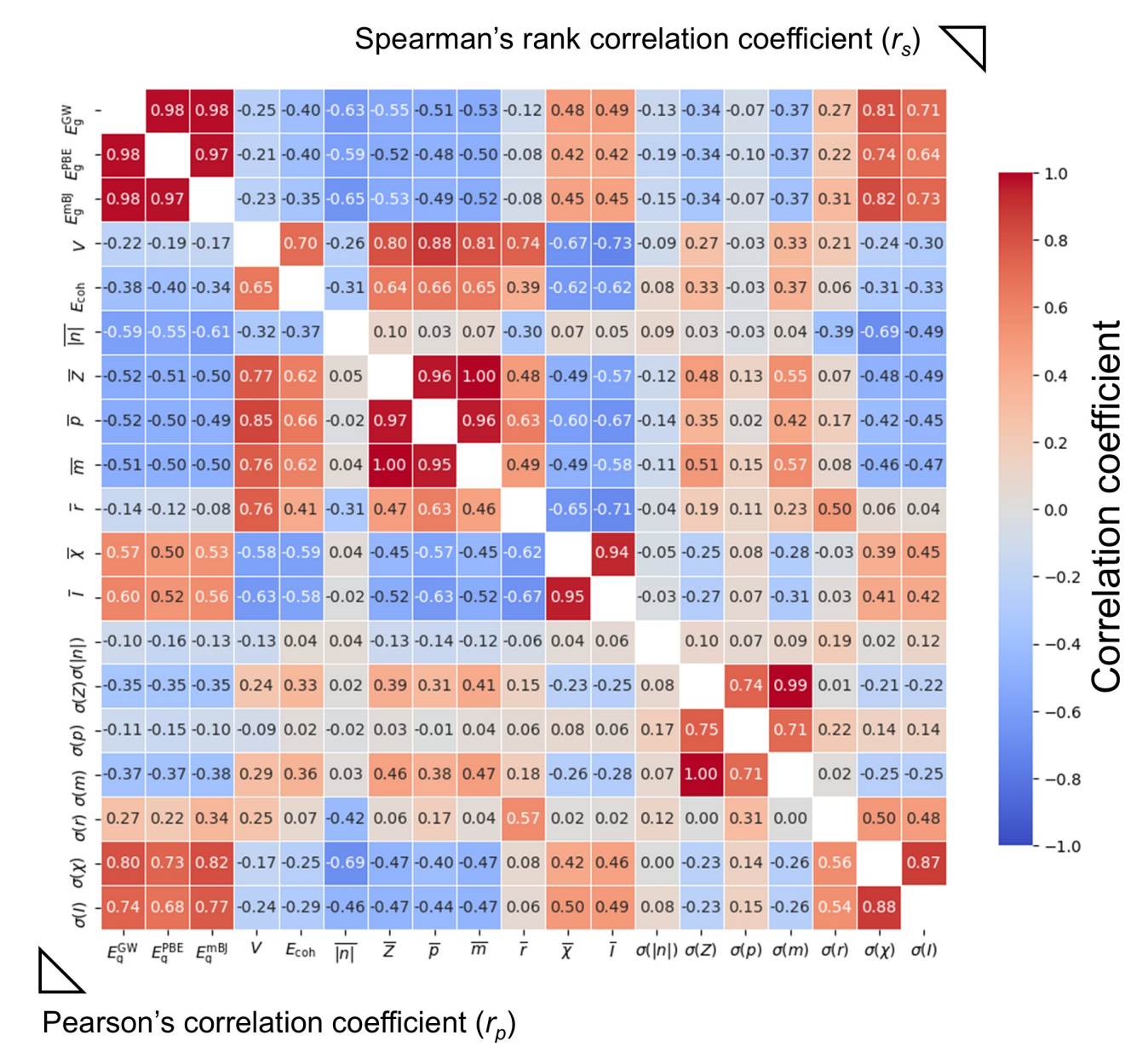


Figure S2. Correlation coefficients for relationship between $E_{\rm g}^{\rm GW}$ and 18 features for 270 binary and ternary inorganic compounds. The left-lower and right-upper triangles represent r_p and r_s , respectively.

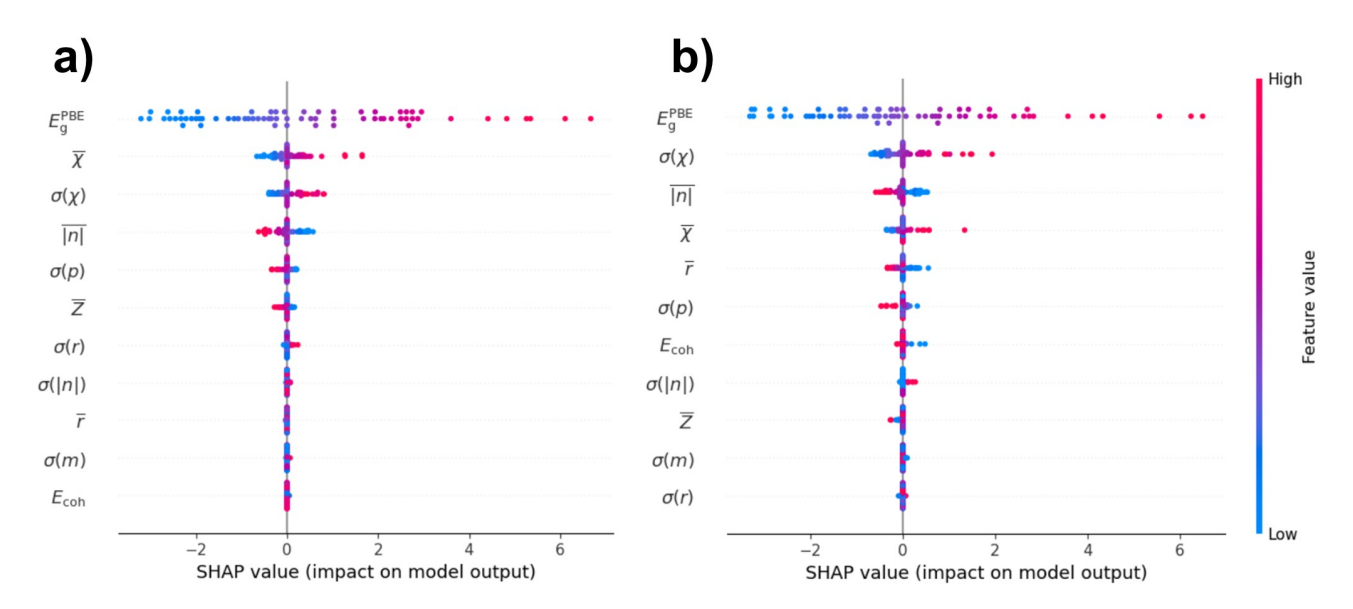


Figure S3. Beeswarm plots from SHAP analysis using SVR model with 11-feature set for predicting $E_{\rm g}^{\rm GW}$. The plots illustrate the relationships between the SHAP values and features in the test dataset, along with their distributions in panels (a) and (b), representing two different data samplings. Notably, for some features with low SHAP importance (indicated by small feature-distribution ranges), the impact of increases or decreases in the feature values on the SHAP values follows different trends for different samples.

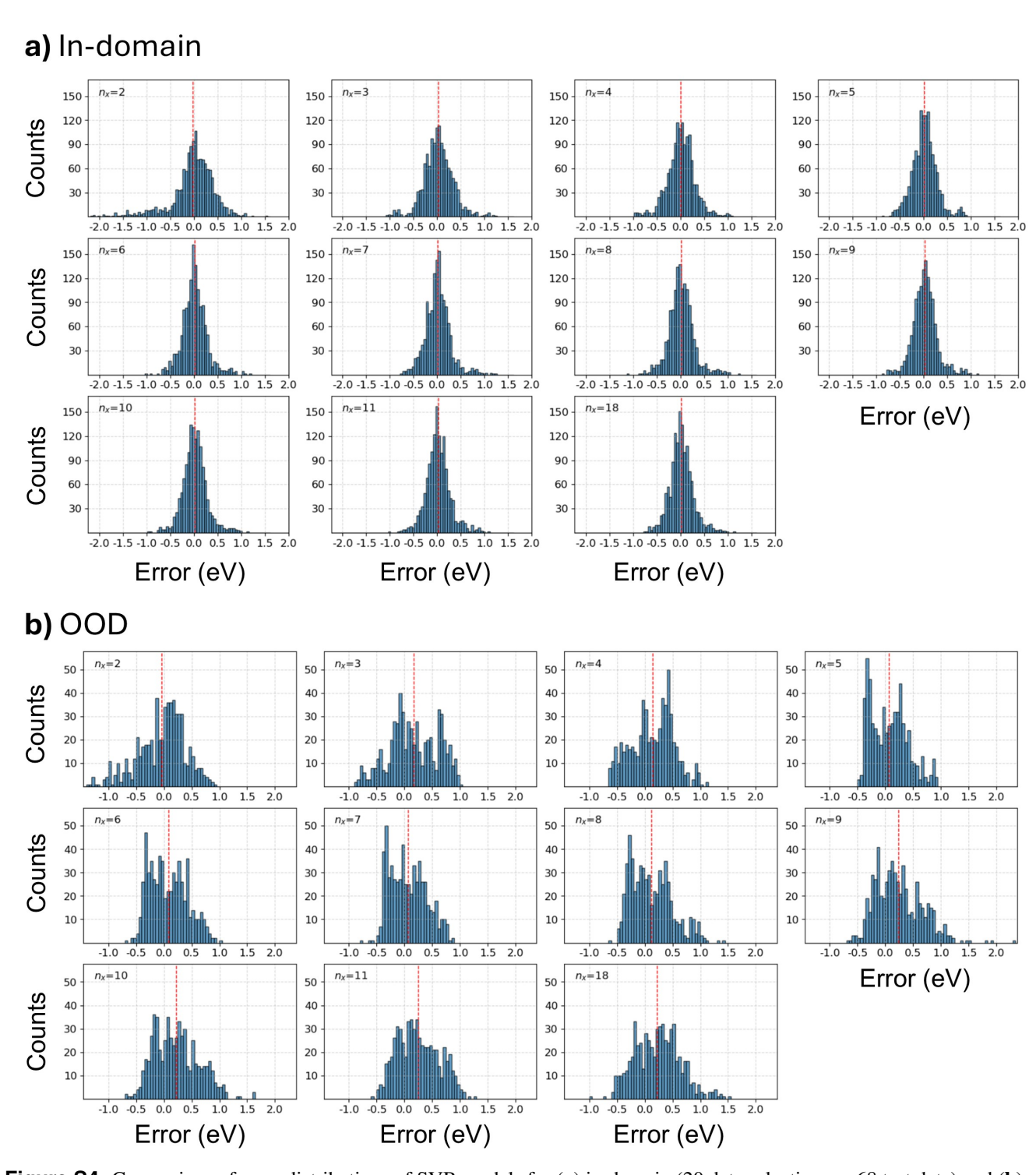


Figure S4. Comparison of error distributions of SVR models for (a) in-domain (20 data selections \times 68 test data) and (b) OOD (20 data selections \times 30 data) data across different number of features. The red, dashed, vertical line indicates the mean of the error distribution for each model.

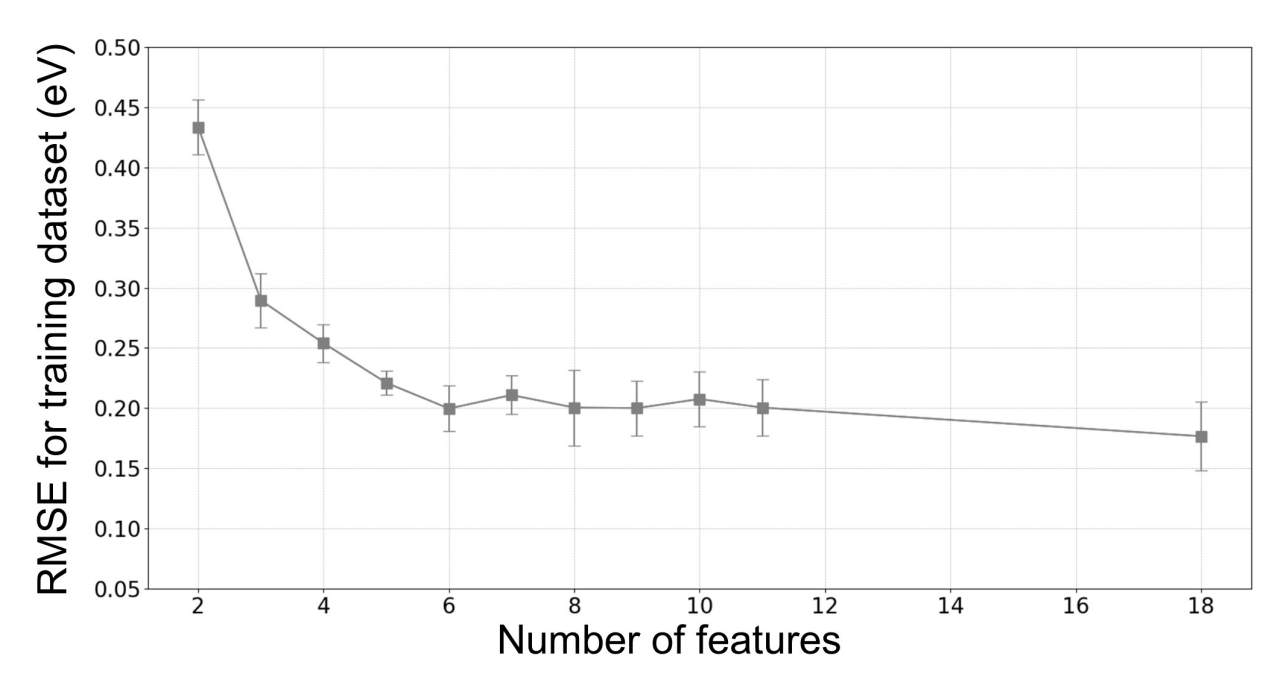


Figure S5. Dependence of RMSE for the training dataset of SVR model on the number of features selected based on XML importance scores. The value at $n_x = 18$ corresponds to the pristine model. The error bars indicate one standard deviation across the predictive models with 20 different data selections.

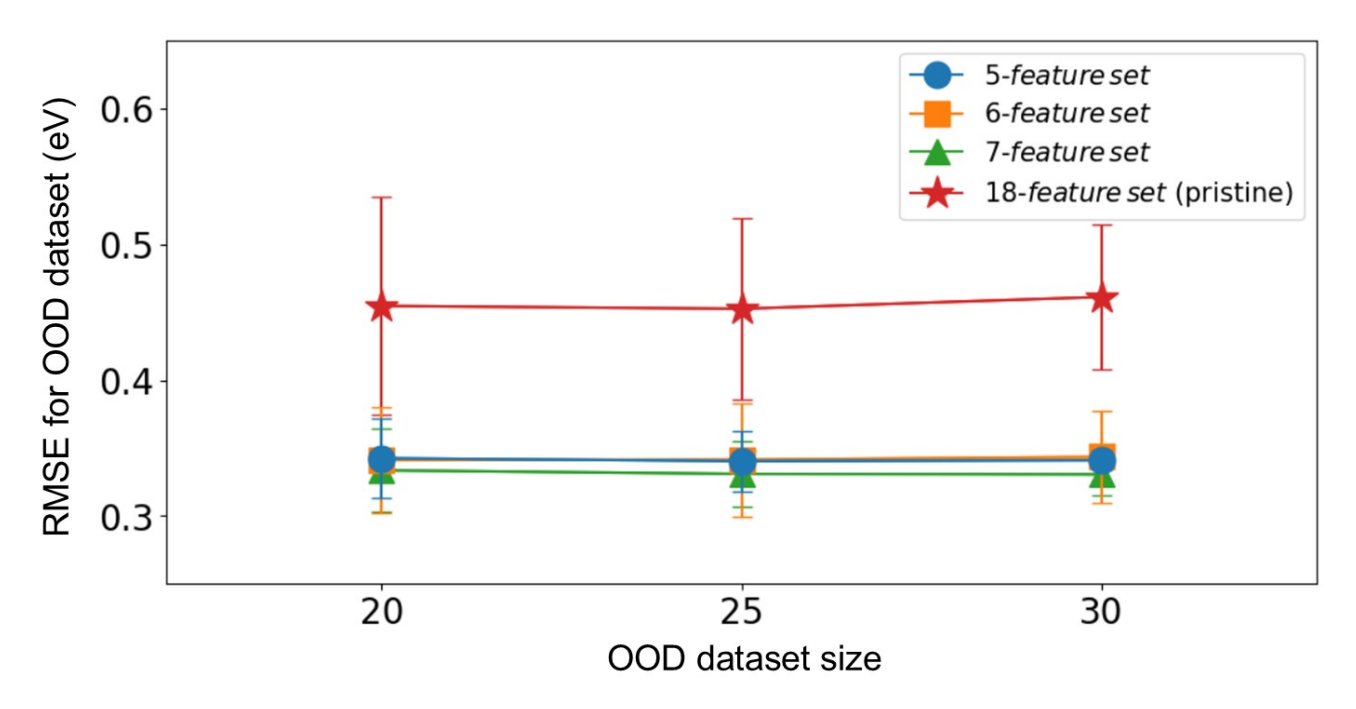


Figure S6. Dependence of RMSE for the OOD dataset on size of OOD dataset. The value at $n_x = 18$ corresponds to the pristine model. The error bars indicate one standard deviation across the predictive models with 20 different data selections.

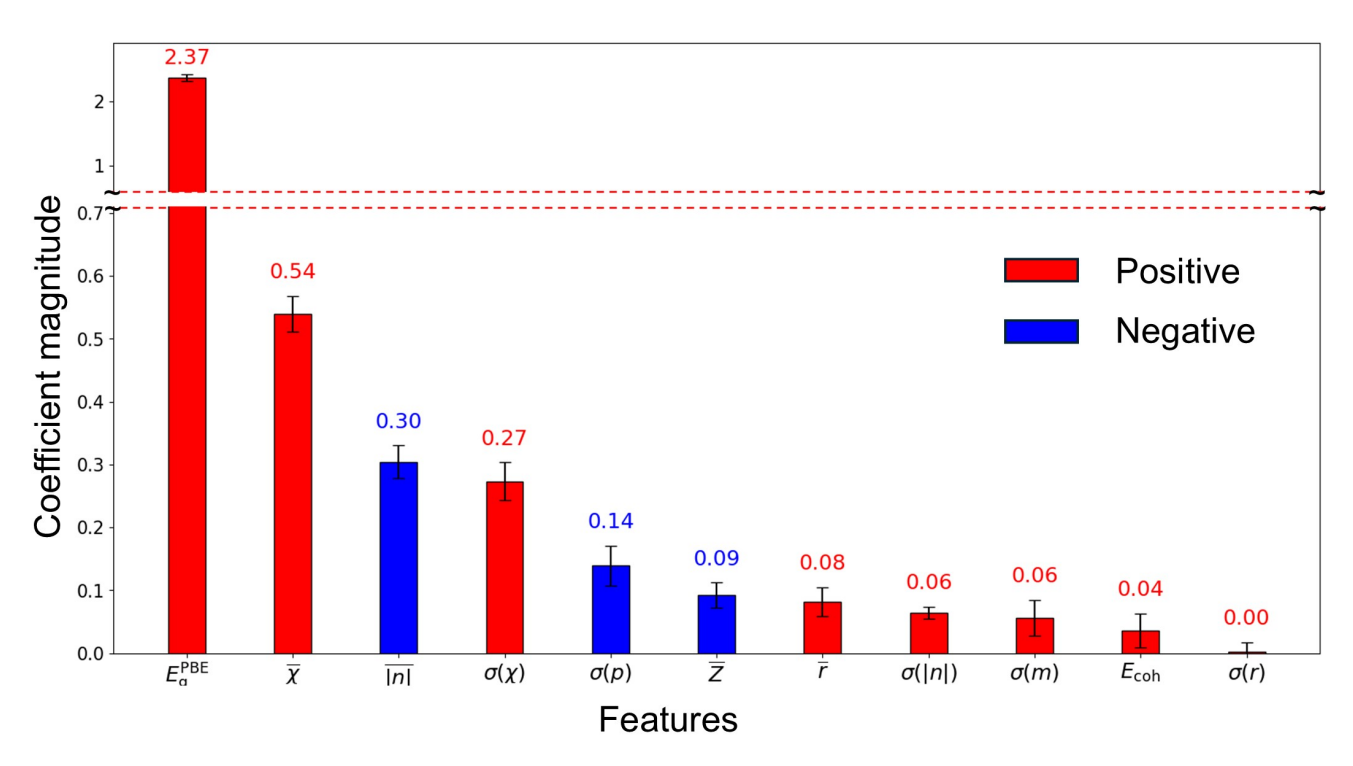


Figure S7. Coefficient magnitudes of LASSO regression models for predicting $E_{\rm g}^{\rm GW}$ using the 11-feature set. The absolute coefficient magnitudes serve as measures of feature importance in LASSO. When the signs of the coefficients are consistently positive or negative across the predictive models using 20 different data selections, the bars are colored red and blue, respectively. The error bars represent one standard deviation of the coefficient magnitudes across the predictive models constructed using 20 different data selections. The horizontal axis indicates the features ranked in descending order of their absolute coefficient magnitudes in the 11-feature model, where the same ordering is used to construct the reduced-feature models with $n_x = 2-11$ in Fig. 2.

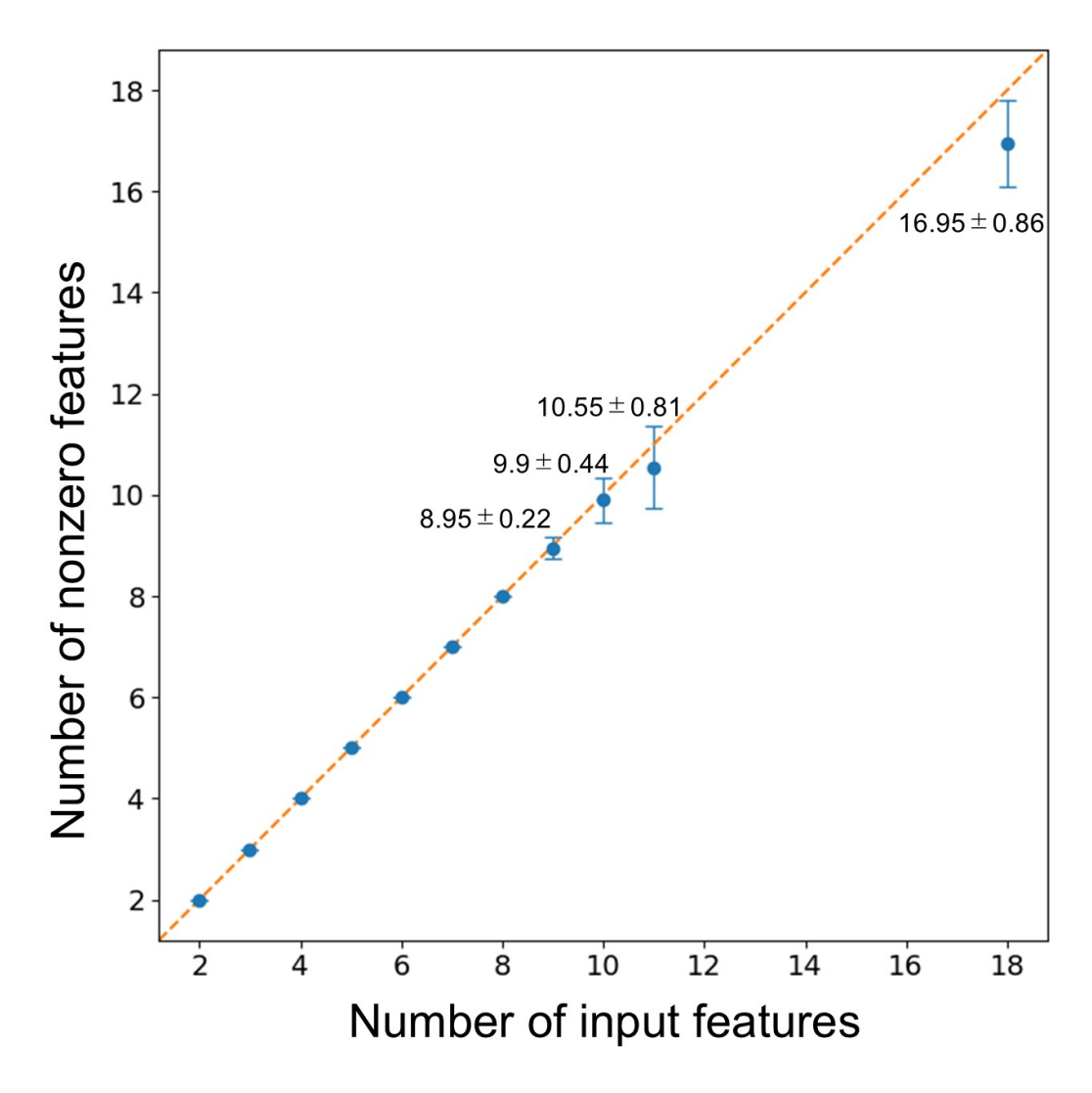


Figure S8. Relationship between the number of input features and the number of nonzero (unshrunk) features in LASSO regression models. Points and error bars represent the mean and one standard deviation obtained using 20 different data selections. For LASSO models with $n_x \le 11$, the input feature subsets are determined based on the feature importance ranking derived from the absolute coefficients of the *11-feature* LASSO model. The diagonal line indicates the case where the number of input and nonzero features are equal.

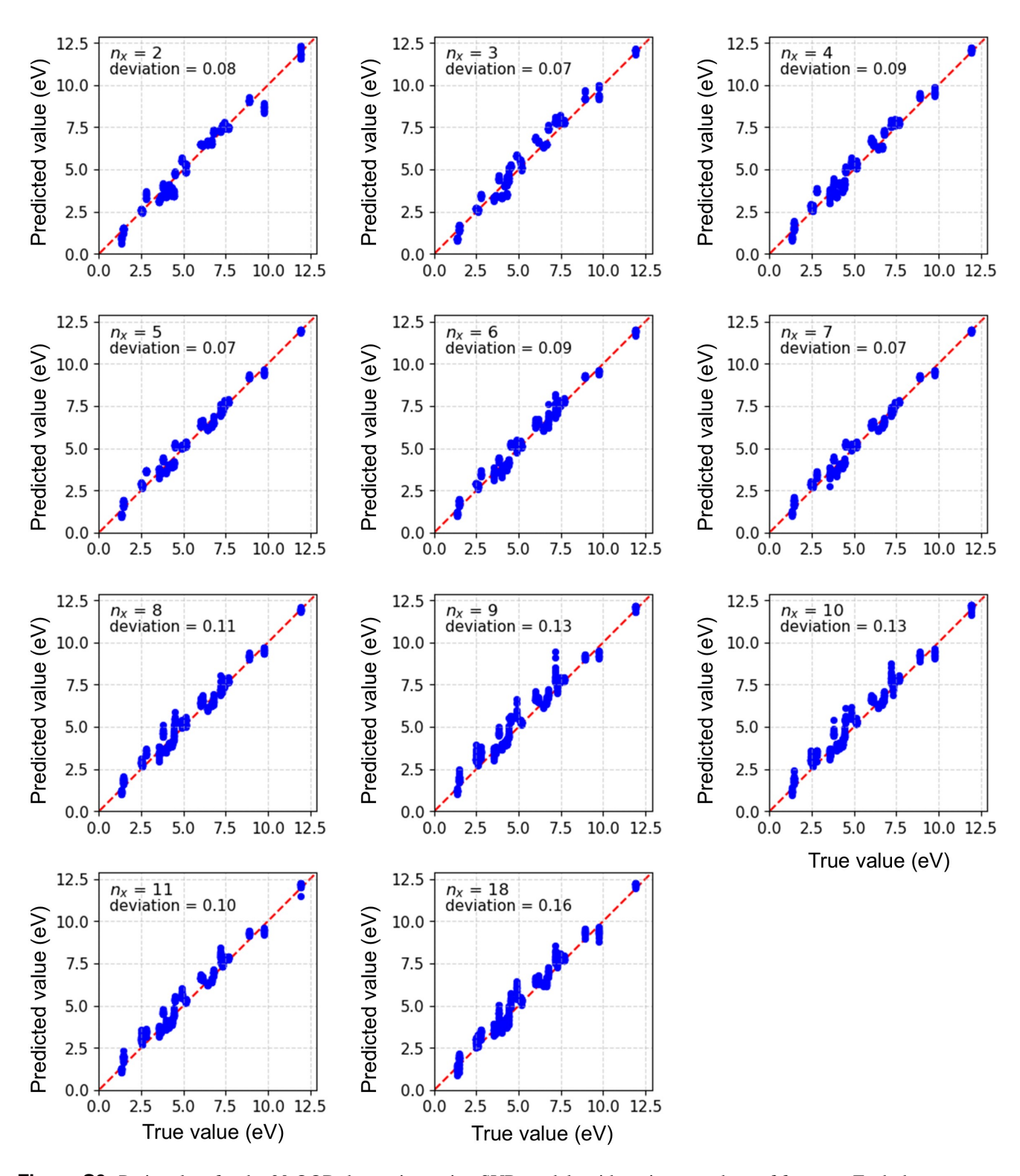


Figure S9. Parity plots for the 30 OOD data points using SVR models with various numbers of features. Each dot represents the predicted values from the predictive models with 20 different data selections. The deviations of these predictions, obtained using equation (4), are also shown in each subplot.

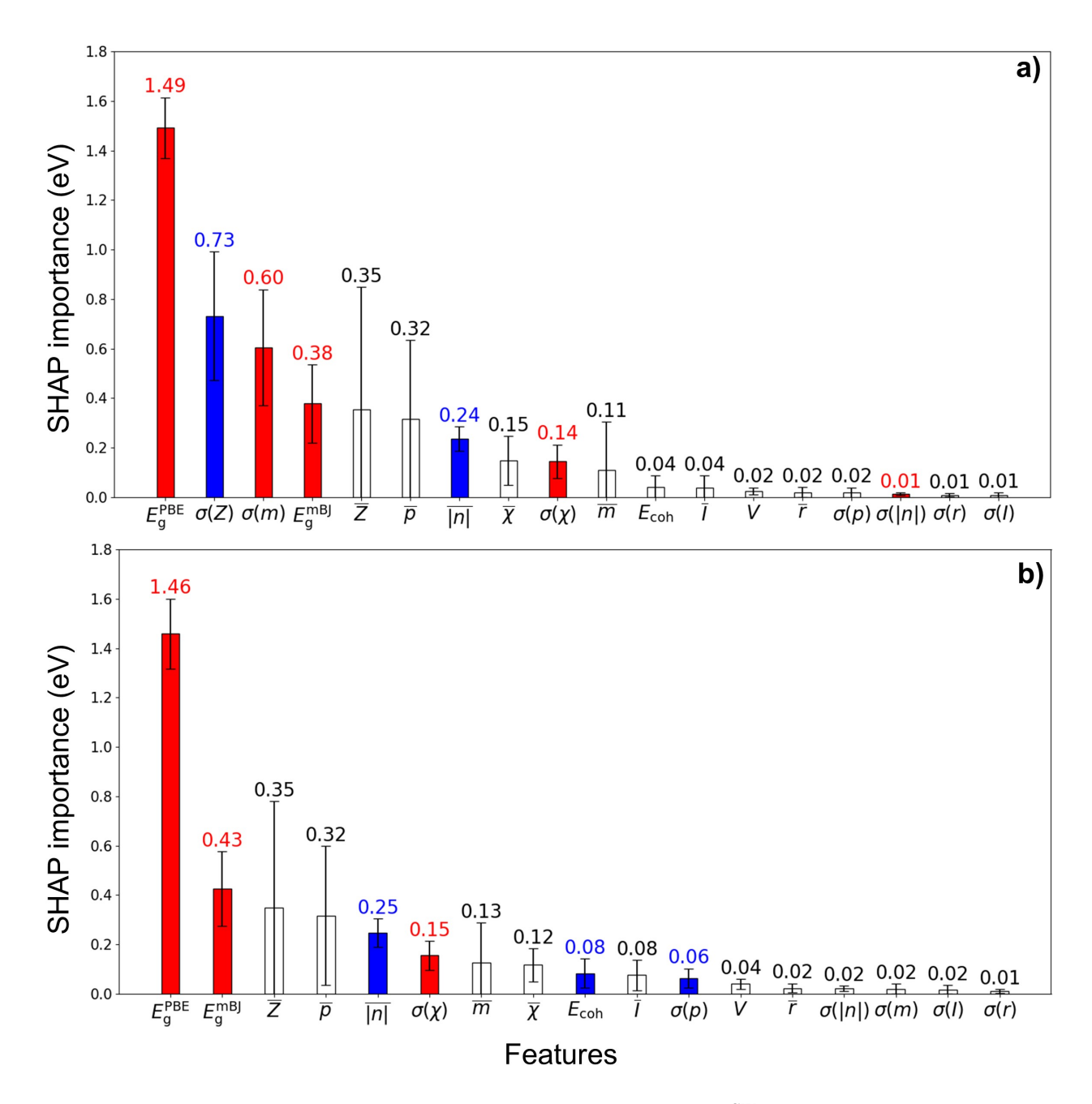


Figure S10. SHAP importance scores for SVR regression models for predicting E_g^{GW} (a) with 18-feature set and (b) with 17-feature set, excluding $\sigma(Z)$. Detailed information relevant to most options such as error bars and colors for the bar graph are presented in Fig. 1.

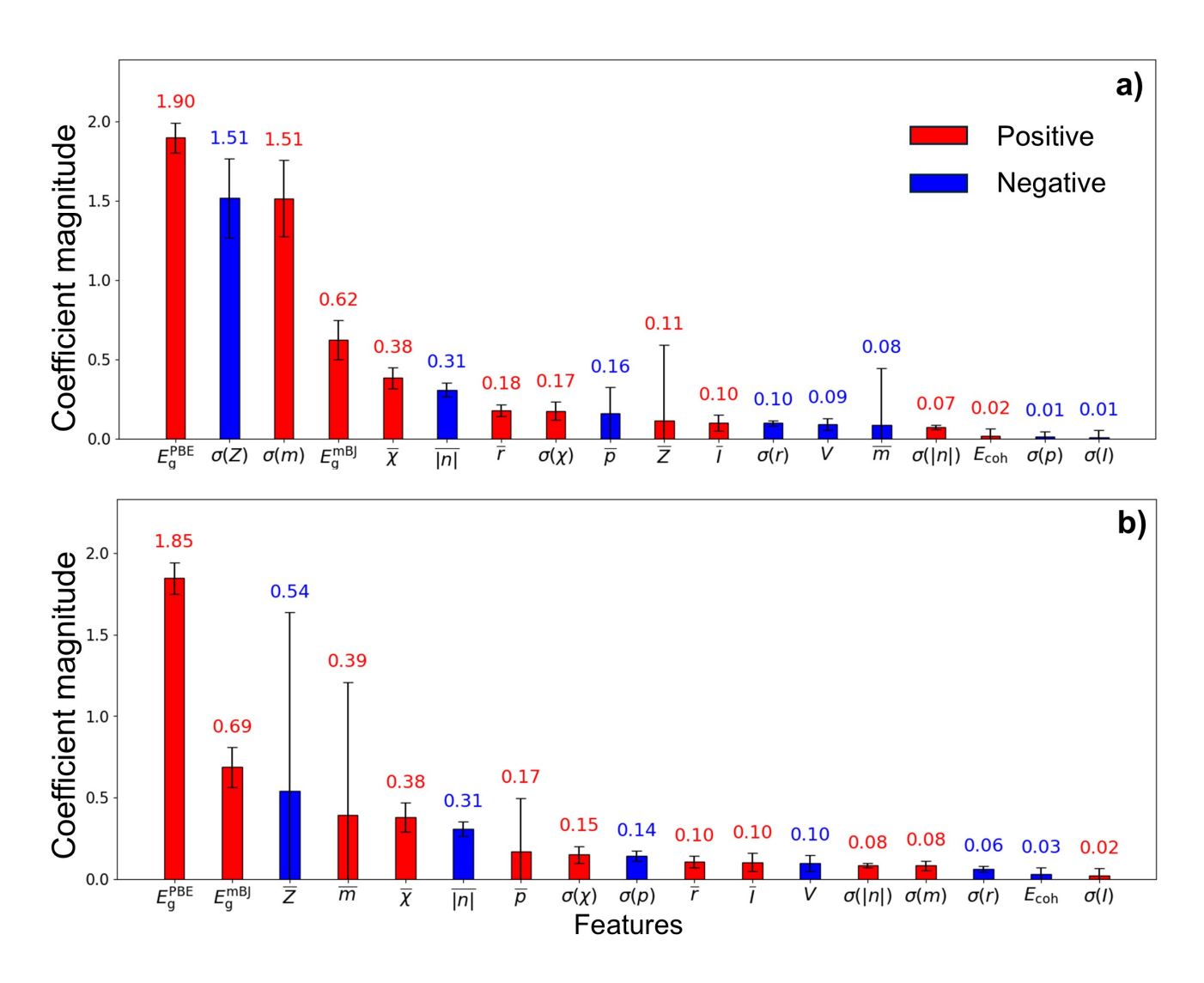


Figure S11. Coefficient magnitudes for LASSO regression models for predicting E_g^{GW} (a) with 18-feature set and (b) with 17-feature set, excluding $\sigma(Z)$. Detailed information relevant to most options such as error bars and colors for the bar graph are presented in Supplementary Fig. S7.

Table S1. Prediction objective $(E_{\rm g}^{\rm GW})$ and 18-feature set for 30 inorganic compounds in the OOD dataset.

7.2957 11.9348 7.6628 3.9671 4.4942 2.5731 9.7422	4.5121 7.0616 4.4997 1.4444	8.1402 11.1670 7.2609	12.9682 13.2148	-6.2480 -4.5830	2.1818 1.2000	16.5455 10.8000	2.8182	37.8710
7.6628 3.9671 4.4942 2.5731	4.4997			-4.5830	1.2000	10 2000		
3.9671 4.4942 2.5731		7 2609					2.5000	22.6175
4.4942 2.5731	1 4444		14.9860	-6.0202	2.2857	11.1429	2.5714	22.5949
2.5731		2.4773	11.2193	-4.0971	1.7143	12.0000	2.4286	27.5813
	2.4086	3.2974	11.0575	-6.6312	2.4000	13.2000	2.8000	27.1916
9.7422	1.3148	1.9023	21.6331	-3.3590	2.0000	34.0000	4.0000	77.9763
	5.7471	8.3629	11.5838	-5.0382	2.0000	10.0000	2.3333	20.1753
3.6427	1.9515	3.0520	20.6793	-3.8678	2.0000	23.0000	3.5000	49.7453
2.4735	1.3589	1.5010	21.9054	-4.0599	2.0000	33.0000	4.1250	74.9235
4.8743	2.8955	5.9543	15.7313	-6.1316	2.4000	27.2000	3.5000	64.2124
7.4352	4.2828	7.7007 5.1058	16.4389	-5.5448	2.0000	16.2857	2.8571	36.0139
6.1561	3.6202		11.0947	-6.5271 -5.8407	2.2857 2.2222	14.8571	2.8571	31.4236 41.1021
5.1163 4.3042	2.7354 1.5673	4.7175 3.0119	14.1686 12.2842	-5.8407 -5.1016	2.4000	18.6667 20.6000	3.1111 3.1000	46.2713
	0.4779	1.0420	19.4042	-3.1010 -3.4389	2.4000	25.2500	3.6250	
1.4490 6.0101	3.6961	4.5151	13.4476	-5.4389 -5.9338	2.4000	21.4000	3.2000	55.0471 47.8970
6.6509	3.5750	4.6381	14.6161	-5.9558 -5.3528	2.4000	15.6667	3.0000	34.0563
5.1504 4.4220	2.5202	4.6497 1.6553	11.7934 12.6273	-4.4159 -6.9179	2.0000	14.7500 17.3333	2.6250 2.8333	32.8801 38.7000
3.5544	1.6060	1.6553 2.9001	36.1526	-6.9179 -1.9795	2.6667 1.1429		5.0000	38.7000 119.3947
	1.7747 3.5351	5.8293	15.0273	-1.9795 -4.2558	1.1429	50.5714	2.8889	35.7296
6.4371 3.7909				-4.2338 -6.5718		16.0000		35.7296
1.3345	1.8501 0.0622	2.7358 0.6795	11.8274 26.0467	-0.5718 -2.9551	2.4000 2.0000	16.8000 38.7500	3.0000 4.3750	91.3709
2.7707	1.4149		21.8604	-2.9331 -3.8344				
	2.2812	2.5868 3.2152		-3.8344 -3.4531	1.5000 2.0000	36.5000	4.2500	85.5215
4.1526	0.5130	0.6041	21.1218		2.0000	18.7500	3.1250	40.7980 93.9974
1.4492 4.3044	1.6193	3.1185	24.4210	-3.4238		39.7500	4.5000 3.0000	
8.9145	5.5435	9.1449	16.5305	-3.3477 -4.6714	1.3333 1.7143	14.3333		30.1040
	4.1321		14.2480 16.0099	-4.6714 -5.6548	2.4000	10.0000 26.8000	2.4286	20.3106
6.7642 7.1743	4.1321	5.9146 5.3508	14.4879	-5.0348 -6.6017	2.4667	24.0000	3.5000 3.1667	63.1304 55.9117
	4.3930 <u>Ī</u>							
$\frac{\bar{\chi}}{2.5282}$	10.5795	$\frac{\sigma(n)}{0.3857}$	$\frac{\sigma(Z)}{18.6809}$	$\frac{\sigma(p)}{1.5266}$	$\frac{\sigma(m)}{47.0025}$	$\frac{\sigma(r)}{0.4314}$	σ(χ)	$\frac{\sigma(I)}{3.4646}$
2.3282	12.4596	0.6000	4.6861	0.8062	9.4045	0.4314	1.0581 1.4465	6.0951
2.5843		0.8806	4.0801	0.8062	9.4043 8.4151	0.4315		3.8299
2.3843	10.4215 8.9775		20.1282	1.1157	50.9776	0.4313	1.0323 1.1945	4.0596
2.5720	10.7591	1.0302 0.8000	6.4000	0.9798	13.9271	0.3439	1.1943	3.5088
2.2488	8.9886	0.8660	22.1980	1.1180	58.0362	0.3439	0.3355	1.3770
2.2466	11.7325	0.4082	3.0822	0.4714	6.3013	0.1404	0.8200	3.0098
2.9330	8.5705	0.7071	13.9104	0.4714	33.6213	0.2237	0.4205	1.8758
2.1730	8.6185	1.2247	3.8079	0.3307	9.8554	0.1293	0.4203	1.1720
2.1873	10.5691	1.2247	24.8548	1.8574	62.8484	0.5007	1.1631	3.7981
2.6600	11.3442	0.9258	13.4453	1.3553	32.0184	0.5711	1.1886	4.4037
2.5129	10.3984	0.4518	10.6962	1.1249	24.9296	0.3475	1.0832	3.7183
2.4744	10.2268	0.4157	12.7976	1.2862	30.3908	0.4019	1.1052	3.7989
2.6400	10.2206	0.9165	16.0947	1.3748	38.9417	0.3867	1.0290	3.5723
2.2275	9.2233	0.8660	10.8022	0.6960	27.0556	0.1433	0.3619	1.1966
2.5920	10.5644	0.9165	16.6565	1.4697	39.7054	0.1433	1.0654	3.7508
2.2683	9.4998	1.0000	10.0303	1.1547	25.6086	0.5533	1.1929	4.1906
2.4275	10.2686	0.8660	15.2541	1.1110	36.0241	0.2588	1.0612	3.5299
2.7967	11.3605	0.9428	18.3182	1.4625	45.5683	0.3609	0.9373	3.2807
2.7907	9.4216	0.3499	2.8212	0.0000	8.7836	0.0789	0.4076	1.2669
2.1522	9.0566	0.9162	13.8724	1.2862	32.5143	0.5887	1.1996	4.2038
2.1322	10.6755	0.8000	11.9063	1.2649	28.2960	0.4006	1.1990	3.6218
1.9688	8.6296	0.8660	14.0601	0.6960	37.8793	0.4000	0.1519	0.6146
2.2400	9.9259	0.5000	16.6508	1.2990	40.9260	0.0482	1.0963	4.4851
4.74(1)								2.0971
								0.8210
1.9863								3.9273
1.9863 1.9663		0.4/14	1.3203					3.8318
1.9863 1.9663 1.9100			5 0000	0.7294	10 2092	() // 16/2		
1.9863 1.9663	8.2636 10.6521 10.6317	0.4518 0.9165	5.0990 23.0729	0.7284 1.8574	10.2983 57.8923	0.4163 0.4888	1.1094 1.1232	3.7671
	1.9863 1.9663	1.98638.62021.96638.2455	1.9863 8.6202 0.8660 1.9663 8.2455 1.2247	1.9863 8.6202 0.8660 14.2719 1.9663 8.2455 1.2247 12.3870 1.9100 8.2636 0.4714 7.5203	1.9863 8.6202 0.8660 14.2719 0.9270 1.9663 8.2455 1.2247 12.3870 0.5000 1.9100 8.2636 0.4714 7.5203 0.8165	1.9863 8.6202 0.8660 14.2719 0.9270 34.0281 1.9663 8.2455 1.2247 12.3870 0.5000 33.8235 1.9100 8.2636 0.4714 7.5203 0.8165 16.8242	1.9863 8.6202 0.8660 14.2719 0.9270 34.0281 0.1293 1.9663 8.2455 1.2247 12.3870 0.5000 33.8235 0.0495 1.9100 8.2636 0.4714 7.5203 0.8165 16.8242 0.4391	1.9863 8.6202 0.8660 14.2719 0.9270 34.0281 0.1293 0.6661 1.9663 8.2455 1.2247 12.3870 0.5000 33.8235 0.0495 0.1572 1.9100 8.2636 0.4714 7.5203 0.8165 16.8242 0.4391 1.1395

^aFrom Materials Project Database. [Jain et al., Appl. Mater. Phys. Lett. 1, 011002 (2013)]

b In the unit of eV.
C In the unit of Å³/atom.
In the unit of eV/atom.

Table S2. Sequential order of elimination of seven features from the pristine 18-feature set prior to XML analyses.

# Features	r_p	r_s	Survived feature			Eliminated feature				<i>p</i> -value (<i>t</i> -test)	
at test			Feature	RMSE (eV) (a)	r_p vs. $E_{\rm g}^{ m GW}$	r_s vs. $E_{\rm g}^{\rm GW}$	Feature	RMSE (eV) (a)	r_p vs. $E_{\rm g}^{ m GW}$	r_s vs. $E_{\rm g}^{\rm GW}$	
18	1.00	1.00	\overline{Z}	0.252	-0.52	-0.55	\overline{m}	0.252	-0.51	-0.53	0.381 ^(c)
17	1.00	0.99	$\sigma(m)$	0.245	-0.37	-0.37	$\sigma(Z)$	0.246	-0.35	-0.34	0.065 (c)
16	0.97	0.97	$E_{\rm g}^{ m PBE}$	0.387	0.98	0.98	$E_{\rm g}^{ m mBJ}$	0.255	0.98	0.98	$< 1 \times 10^{-10} \ ^{(b)}$
15	0.97	0.96	$\overline{\overline{Z}}$	0.262	-0.52	-0.55	$\frac{\varepsilon}{p}$	0.263	-0.52	-0.51	0.020 ^(c)
14	0.95	0.94	$\overline{\chi}$	0.268	0.57	0.48	$ar{I}$	0.251	0.60	0.49	0.001 (b)
13	0.88	0.87	$\sigma(\chi)$	0.271	0.80	0.81	$\sigma(I)$	0.258	0.74	0.71	0.007 (b)
12	0.77	0.80	\overline{Z}	0.252	-0.52	-0.55	V	0.255	-0.22	-0.25	0.257 ^(c)
11	0.73 ^(d)	0.74 ^(d)	$E_{ m g}^{ m PBE}$	0.960	0.98	0.98	$\sigma(\chi)$	0.289 ^(d)	0.74	0.71	$< 1 \times 10^{-15}$

^aThe RMSE obtained using the predictive model when this feature is removed. ± indicates one standard deviation across the predictive models with 20 different data selections.

 $[^]b$ The elimination is based on a statistically significant increase (99% confidence level) in the prediction error (p-value < 0.01). c The elimination is based on lower correlation with the prediction objective ($E_{\rm g}^{\rm GW}$) as no significant error difference is observed (p-value > 0.01).

^dWhen the threshold for elimination based on the correlation is set below 0.8, an additional feature pair is tested for removal. For this pair, elimination of either feature leads to a sharp increase in the prediction error, indicating that both features are required for accurate prediction. Therefore, the feature elimination process is terminated at this point.

Table S3. Prediction errors for test dataset using SVR models with different numbers of features. \pm indicates one standard deviation across the predictive models with 20 different data selections.

Number of		In-domain		OOD			
features	RMSE (eV)	MAE (eV)	\mathbb{R}^2	RMSE (eV)	MAE (eV)	\mathbb{R}^2	
18	0.247 ± 0.019	0.184 ± 0.013	0.993 ± 0.001	0.461 ± 0.053	0.374 ± 0.042	0.974 ± 0.006	
11	0.255 ± 0.025	0.188 ± 0.018	0.993 ± 0.001	0.441 ± 0.039	0.352 ± 0.027	0.978 ± 0.005	
10	0.256 ± 0.025	0.189 ± 0.015	0.993 ± 0.001	0.452 ± 0.079	0.359 ± 0.054	0.974 ± 0.011	
9	0.253 ± 0.021	0.186 ± 0.014	0.993 ± 0.001	0.470 ± 0.109	0.367 ± 0.068	0.972 ± 0.014	
8	0.266 ± 0.031	0.195 ± 0.017	0.992 ± 0.002	0.386 ± 0.038	0.308 ± 0.030	0.978 ± 0.004	
7	0.260 ± 0.025	0.189 ± 0.016	0.993 ± 0.002	0.331 ± 0.016	0.275 ± 0.012	0.983 ± 0.002	
6	0.259 ± 0.026	0.189 ± 0.016	0.993 ± 0.002	0.344 ± 0.033	0.287 ± 0.029	0.982 ± 0.003	
5	0.254 ± 0.020	0.191 ± 0.014	0.993 ± 0.001	0.341 ± 0.008	0.283 ± 0.008	0.982 ± 0.001	
4	0.289 ± 0.021	0.217 ± 0.015	0.991 ± 0.002	0.405 ± 0.023	0.338 ± 0.019	0.978 ± 0.001	
3	0.312 ± 0.032	0.234 ± 0.023	0.989 ± 0.003	0.467 ± 0.027	0.380 ± 0.021	0.972 ± 0.001	
2	0.453 ± 0.045	0.313 ± 0.033	0.978 ± 0.004	0.432 ± 0.020	0.336 ± 0.016	0.971 ± 0.002	